Clinical/Basic Science Research Article

OTA INTERNATIONAL
www.otainternational.org

OPEN

3D printed titanium cages combined with the Masquelet technique for the reconstruction of segmental femoral defects

Preliminary clinical results and molecular analysis of the biological activity of human-induced membranes

Kevin Tetsworth, MD, FRACS[a,b], Anna Woloszyk, PhD[c], Vaida Glatt, PhD[b,c,*]

Abstract

Introduction: Traumatic femoral segmental bone loss is a complex clinical problem, one that often requires extreme solutions. This study examines a new treatment strategy for segmental bone loss using patient-specific 3D printed titanium cages in conjunction with the Masquelet technique.

Methods: The study was composed of a clinical observational case series, and a basic science investigation to evaluate the biological activity of the induced membranes using histology, immunohistochemistry (IHC), and gene expression analysis. Eligible patients were: adult; post-traumatic; with segmental femoral defects; minimum follow-up 1 year; managed under a 2-stage protocol, with an interim antibiotic poly (methyl methacrylate) (PMMA) spacer. Definitive reconstruction was completed with exchange to a 3D printed custom titanium cage filled with bone graft, and stabilized with either an intramedullary (IM) nail or a lateral locked plate.

Results: Patient-specific 3D printed titanium cages were used in 5 consecutive patients to reconstruct post-traumatic segmental femoral defects. The mean interval between stages was 100.2 days (83–119 days), the mean defect length was 14.0 cm (10.3–18.4 cm), and the mean bone defect volume measured 192.4 cc (114–292 cc). The mean length of follow-up was 21.8 months (12–33 months). There were no deep infections, fractures, nerve injuries, loss of alignment, or nonunions identified during the period of follow-up. All of the patients achieved union clinically and radiographically. Histology and IHC demonstrated a greater number of vessels, cell nuclei, and extensive staining for cluster of differentiation 68 (CD68), platelet and endothelial cell adhesion molecule 1 (PECAM-1), and vascular endothelial growth factor (VEGF) in the induced membranes compared to local fascia controls. Gene expression analysis revealed significant differential regulation of essential genes involved in inflammatory, angiogenic, and osteogenic pathways [interleukin 6 (IL-6), nuclear factor kappa B1 (NF-κB1), receptor activator of nuclear factor kappa-β ligand (RANKL), vascular endothelial growth factor A (VEGFA), angiogenin (ANG), transforming growth factor, beta 1 (TGF-β1), bone morphogenetic protein-2 (BMP-2), growth differentiation factor 5 (GDF-5), growth differentiation factor 10 (GDF-10), and runt-related transcription factor 2 (RUNX-2)] in the induced membranes.

Conclusions: This study demonstrates that the use of a patient-specific 3D printed custom titanium cage, inserted into an induced membrane in a 2-stage protocol, can achieve very acceptable clinical outcomes in selected cases of post-traumatic femoral segmental defects. Patient-specific 3D printed titanium cages, used in conjunction with the Masquelet technique, are a promising new treatment option for managing complex trauma patients with femoral bone loss.

Level of Evidence: Level IV (observational case series).

Keywords: 3D modeling, 3D printing, biomembranes, bone regeneration, gene expression, histology, induced membranes, limb salvage, Masquelet technique, open fractures, osteogenesis, segmental bone defects

The authors have no funding and no conflicts of interest to disclose.

[a] Royal Brisbane and Women's Hospital, Herston, Queensland, [b] Orthopaedic Research Centre of Australia, Brisbane, Queensland, Australia, [c] Department of Orthopedic Surgery, University of Texas Health Science Center San Antonio, Texas

[*] Corresponding author's address: Department of Orthopedic Surgery, University of Texas Health Science Center San Antonio, 7703 Floyd Curl Drive—MC 7774, San Antonio, Texas 78229-3900. Tel: +210 450 8094.
E-mail address: glatt@uthscsa.edu (V. Glatt).

OTA (2019) e016

Received: 15 April 2018 / Accepted: 24 September 2018

http://dx.doi.org/10.1097/OI9.0000000000000016

1. Introduction

Traumatic segmental bone loss is a complex clinical problem, one that often requires extreme solutions.[1] Options for management include Ilizarov methods,[2,3] microvascular free fibular transfer,[4,5] massive bone grafts,[6] amputation,[7] the Masquelet technique,[8–11] or arthroplasty with mega-prostheses.[12] Joint and limb preserving treatments are preferred in younger patients, using techniques that are mechanically robust enough to allow early motion and mobilization. Improving our ability to successfully manage these injuries is critically important, as they often result in a protracted course of continued medical care that is inevitably costly, with a significant risk of arthrodesis or amputation of the involved limb.[1,7,13]

The Masquelet technique has rapidly gained popularity over the past decade.[8–11] Although touted by some as a revolutionary strategy,[14] others have reported frequent complications and a significant failure rate.[15] Questions still remain in terms of

optimizing the technique, particularly with respect to the timing of the second stage. Although some have suggested the success of the method is independent of the magnitude of bone loss,[8] Mühlhausser et al.[16] identified an increased risk of treatment failure for defects exceeding 80 cc in volume. This is consistent with the outcomes using all other methods, as defects exceeding 8 cm in length are less likely to achieve union regardless of how the defect is managed.[13]

Patient-specific 3D printed titanium cages are a novel means to manage the extremely difficult problem of post-traumatic bone loss. These implants are designed in a virtual surgical procedure that provides a patient-specific option for re-alignment and length correction.[17] Prior studies have reported positive outcomes with limited clinical experience using titanium spinal cages for this purpose, either directly[18–21] or as a staged procedure into an induced membrane.[22] In a series of papers, Lindsey, Gugala and colleagues reported their early experience using titanium spinal cages to support massive cancellous bone grafts when reconstructing large segmental defects.[18–20] O'Malley and Kates[22] were the first to describe the hybrid technique, a single case where a titanium cage was used during a 2-stage reconstruction into an induced membrane. The surgical technique employed here is a further evolution of these concepts, with the added benefit of rapid prototyping and customization of the cage using additive manufacturing technology.[17]

The main purpose of this study was to report the preliminary results in a small clinical series using patient-specific 3D printed titanium cages in conjunction with the Masquelet technique for the reconstruction of massive segmental femoral defects. This study was designed as an observational cohort of traumatic or post-traumatic femoral bone defects, all managed under a common staged protocol. This included a first stage with an antibiotic PMMA spacer utilizing the Masquelet technique,[8–11] followed by a second stage for insertion of a patient-specific 3D printed titanium cage incorporating bone graft.[17] The principal aim was to assess the clinical utility of this approach, and the cumulative complication rate served as the primary outcome measure. As a preliminary investigation of efficacy, routine radiographs and clinical results served as secondary outcome measures. A further aim was to conduct a molecular analysis of the biological activity of the induced membranes,[23–25] and its potential influence on the healing process in massive bone defects.

2. Methods

The study was composed of 2 related components, a clinical observational case series and a concurrent basic sciences investigation to evaluate the induced membranes using histology, IHC, and gene expression analysis. The institutional Human Research Ethics Committee granted approval, and informed consent to participate was obtained from all eligible patients before enrolment.

2.1. Clinical study

Inclusion criteria: adult patients (age >18 years); post-traumatic femoral bone loss; reconstruction under a staged protocol using a 3D printed custom titanium cage.[17] Exclusion criteria: unable or unwilling to consent to participate in the study; length of follow-up < 1 year. The medical records and radiographs of all eligible patients managed at our institution with patient-specific 3D printed titanium cages were evaluated, documenting demographic data and complications. The neurologic status and the presence or absence of infection of the affected limb was ascertained on clinical grounds during follow-up outpatient visits. Local or systemic signs of infection, including persistent erythema, active drainage, wound dehiscence, or positive cultures were all considered adequate for diagnosis. Digital radiographs obtained during routine clinical follow-up were assessed retrospectively after union was achieved, using the measurement tools of the IMPAX (AGFA HealthCare, Greenville, SC) radiology imaging software package. Residual deformity (angulation and translation) was analyzed on routine radiographs in both the coronal and sagittal plane by a single observer (KT). Three measurements were made on each image, with high and low values ignored.

All patients with femoral segmental bone loss underwent 2 operative procedures as part of this treatment strategy (Fig. 1). The initial operation involved resection of all compromised avascular bone fragments and insertion of an antibiotic (vancomycin) PMMA (Palacos R+G containing gentamycin; Heraeus Medical, Hanau, Germany) spacer, stabilized with a plate or IM nail (Fig. 1A–E). This maintained skeletal length and soft tissue tension, facilitating mobilization and rehabilitation. The spacer also allowed for induction of a biologically active membrane, following the Masquelet technique. Stable fixation was achieved with either an IM nail or lateral locked plate, as dictated by clinical considerations. Pathogen-specific antibiotics were continued for at least 6 weeks postoperatively for actively infected cases. High-resolution computed tomography (CT) scans of these temporary constructs were used for planning definitive reconstruction, involving a virtual surgical planning session (Fig. 1F–H).[17]

During the planned second stage procedure, approximately 14 weeks after the first stage, the induced membrane was isolated, split longitudinally, the PMMA spacer removed, and custom 3D printed titanium cages (4Web Medical; Frisco, TX) were implanted into the segmental defect within the induced membrane. The cages were 3D printed from titanium alloy using the CT scan data, mirroring the anatomical contours of the intact opposite limb.[17] The surgeon was involved in the process of designing the implant, so that the planned surgical approach, screw trajectories, plate constructs, and IM devices were all incorporated into the design (Fig. 1F–H).[17] The cage design provides enough strength and stability to permit early motion and protected weight bearing. Autologous bone graft was harvested from either the anterior iliac crest, or from the contra-lateral femur using the reamer-irrigator-aspirator system (Depuy Synthes, Oberdorf, Switzerland). The graft volume required was always very large (exceeding 100 cc in every case), and was therefore augmented as necessary with allograft cancellous chips to achieve adequate volume. Bone graft was digitally impacted into the substance of the cage, and the remaining graft was used liberally at the host-implant junction proximal and distal. Revision fixation was performed as necessary, involving either exchange nailing or modification of the original plates and screws (Fig. 1I–J). The induced membrane was then carefully closed over the construct containing the bone graft to restore the favorable biological milieu. Unrestricted range of motion exercises were begun immediately, progressing as patient comfort allowed. Partial weight bearing (maximum 35 kg) was allowed for 6 weeks, with progression to full weight bearing over the ensuing 6 weeks. Routine clinical care ensued, with radiographs at weeks 0, 6, 12, 26, and 52 (Fig. 1K–O); a CT scan was obtained between 9 and 12 months following completion of the second stage (Fig. 2A–E).

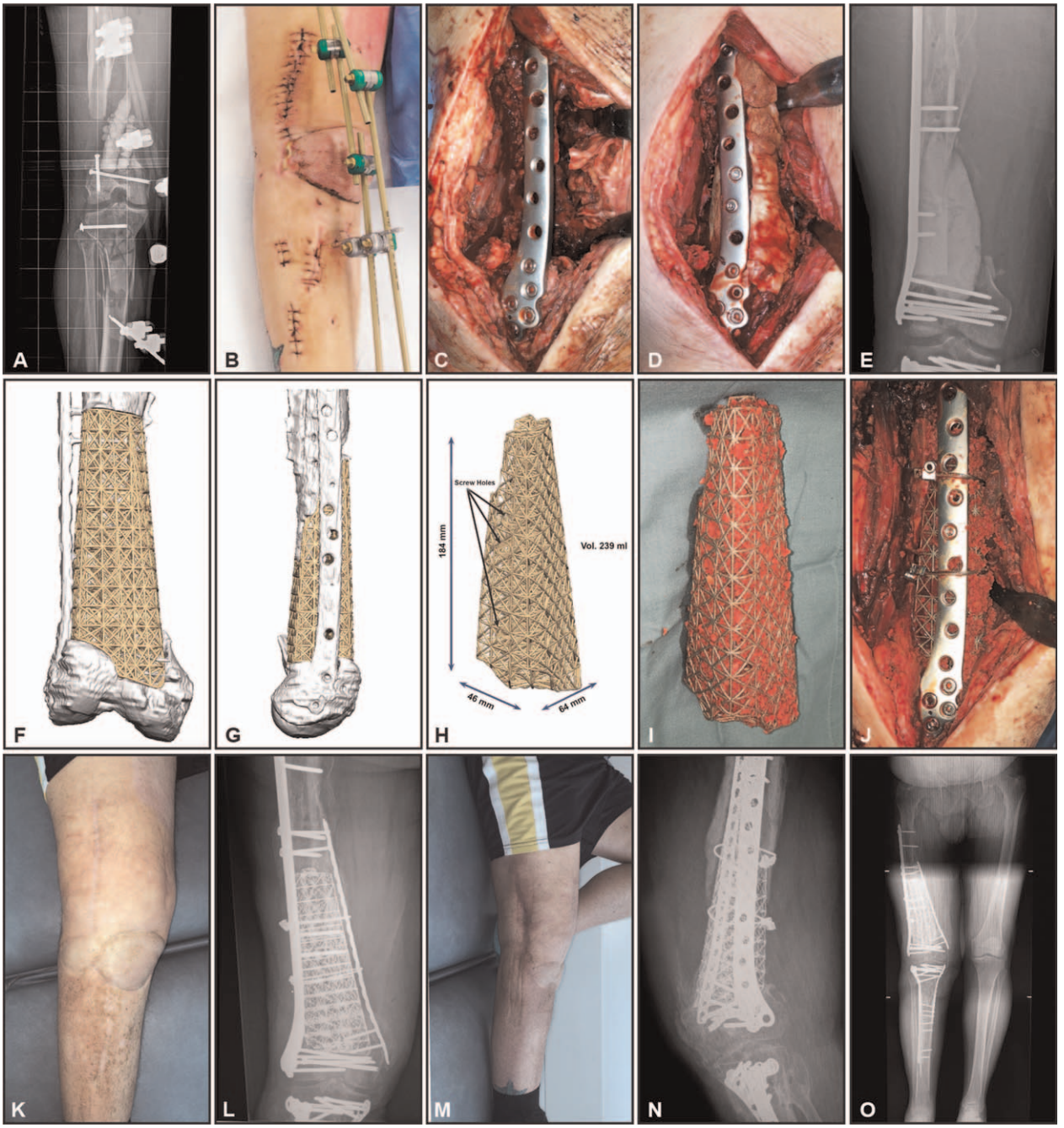

Figure 1. Intrahospital transfer of a 56 year old man with past medical history of smoking and obesity, who sustained polytrauma riding a motorbike struck by a pickup truck in regional Australia. His orthopaedic injuries were largely restricted to a right "floating knee". These fractures included: (i) closed metadiaphyseal fracture of the right proximal tibia with intra-articular extension; (ii) a comminuted right patellar fracture; and (iii) a high-energy Gustilo grade 3B open intra-articular fracture of the right distal femur with segmental bone loss and absent cartilage. (A) Anterior-posterior radiograph following emergency irrigation and debridement, limited screw fixation of intra-articular elements, and spanning external fixation locally before transfer to tertiary care facility; (B) open wound overlying right knee urgently covered with a medial gastrocnemius rotational myoplasty, seen here 3 weeks later; (C) intraoperative photograph of the 15 cm segmental defect after further debridement, return to length, and stabilization with a lateral locked plate; (D) intraoperative photograph of an antibiotic loaded PMMA spacer used to temporarily reconstruct the defect, a variation of the Masquelet technique; (E) Postoperative anterior-posterior radiograph of the temporary construct, with a lateral locked plate and PMMA antibiotic spacer in situ; (F) anterior view of the design proposed for a truss-type titanium cage to reconstruct this defect; (G) lateral view of the design proposed for this truss-type titanium cage implant; (H) detailed specifications for the truss-type titanium cage, 18.4 cm in length after allowing for additional bone resection to enhance the stability of the construct; (I) intra-operative view of the 3D printed patient-specific titanium cage, packed with morselized allogeneic and autograft cancellous bone; (J) intraoperative photograph of the definitive reconstruction of the defect, demonstrating modification of internal fixation with addition of cables and a medial plate not visible here; (K) clinical photograph of the right knee and lower extremity 10 months postoperative, demonstrating benign appearance of the flap; (L) Anterior-posterior radiograph of the right distal femur 10 months postoperative, demonstrating the medial plate further augmenting stability; (M) clinical photograph of the right knee and lower extremity 10 months postoperative, demonstrating small flexion contracture; (N) lateral radiograph of the right distal femur 10 months postoperative; (O) long-standing radiograph of both lower extremities 10 months postoperative, demonstrating 2.2° valgus and a residual 23 mm limb length discrepancy (LLD). Patient's clinical outcome was the most inferior in this series, with a final range of motion of the knee of only 10–75°. Patient's age, patella fracture, loss of articular cartilage, the need for soft tissue coverage with a flap, and the severity of the injuries sustained almost certainly all contributed to the sub-optimal outcome achieved.

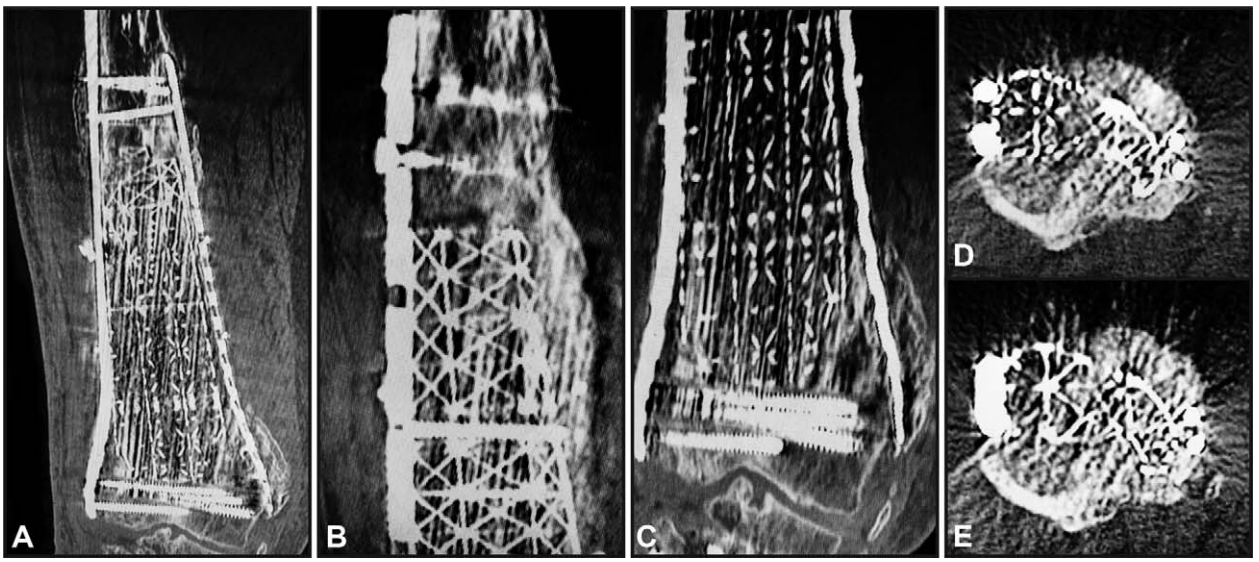

Figure 2. CT scan images obtained at 9 months postoperative of the same patient as depicted in Figure 1. (A) Coronal plane image through the distal femur and central portion of the titanium cage, in the same plane as the 2 plates present medial and lateral. Metal artifact obscures much of the detail with respect to bone growth in the substance of the cage; this artifact is less pronounced at the proximal and distal ends of the implant. (B) Detail of the coronal image through the proximal end of the cage, illustrating bone infiltrating the cage most evident along the medial border. (C) Detail of the coronal image through the distal end of the cage, illustrating mature callus enveloping the medial plate. (D and E) Axial slices through the proximal end of the cage, demonstrating bone penetrating the cage and confirming osseointegration of the implant at these levels, most evident anteromedial and posteriorly.

2.2. Histological analysis

Samples were harvested from the induced membrane and local fascia (control) during the second stage surgical procedure. Specimens were approximately 10×30 mm in size, with 10×20 mm of this used for histology and IHC. After harvest, all specimens were rinsed in PBS and fixed in 4% paraformaldehyde for 48 to 72 hours, depending on the thickness of the sample, at 4°C. Tissue samples were decalcified in 10% EDTA for 10 days on a shaker at room temperature, before being embedded in paraffin, and sectioned at 5 μm. The samples were stained with Hematoxylin & Eosin (H&E) and Masson Trichrome to determine tissue morphology. IHC was performed using anti-CD68 antibody (1:100, ab955, Abcam plc, Cambridge, UK), anti-PECAM-1 (1:100, sc-376764) or anti-VEGF (1:200, sc-7269) (Santa Cruz Biotechnology, Inc., Dallas, TX). Antigens were retrieved using Proteinase K and the sections were incubated in primary antibody dilutions overnight at 4°C. The Mouse and Rabbit Specific HRP (ABC) Detection IHC kit (Sigma-Aldrich Co., St. Louis, MO) in combination with the ImmPACT NovaRED Peroxidase (HRP) Substrate (Vector Laboratories, Inc., Burlingame, CA) was used for antibody detection before the sections were counterstained with 10% hematoxylin.

2.3. Analysis of cell density

Sections mounted with DAPI-Fluoromount-G™ Clear Mounting Media (Southern Biotech, Birmingham, AL) were used to compare the average cell density based on DAPI-stained cell nuclei found in both induced membrane and control samples. Five representative images per sample were acquired at 20× magnification, and the number of cell nuclei per image was analyzed using ImageJ (National Institutes of Health, Bethesda, MD).

2.4. Gene expression analysis

The remaining 10×10 mm portion of the tissue samples were designated for gene expression analysis, preserved in RNA*later*™ (Invitrogen, Thermo Fisher Scientific, Inc., Waltham, MA), and subsequently stored at −80°C. RNA was extracted using the RNeasy Mini Kit (Qiagen, Inc., Germantown, MD) before being transcribed into cDNA (TaqMan High-Capacity RNA-to-cDNA Kit, Applied Biosystems, Thermo Fisher Scientific, Inc., Waltham, MA). Quantitative real-time PCR (qRT-PCR) was performed using a customized TaqMan gene expression PCR array according to the manufacturer's protocol. Expression levels were calculated by the comparative C_T method ($\Delta\Delta C_T$ method) after being normalized to the C_T-value of a housekeeping gene. Fold differences were expressed as a range, where the minimum is $2^{-\Delta\Delta CT+s}$ and the maximum is $2^{-\Delta\Delta CT-s}$, with s being the standard deviation of the $\Delta\Delta C_T$ value. A fold change of >2 or <0.5 was considered significant ($P < .05$).

2.5. Statistics

Data are presented as the mean ± standard deviation (SD). For comparisons between 2 groups, a 2-tailed Student's *t*-test was performed using GraphPad Prism v6.05 (GraphPad Software, Inc., La Jolla, CA). Differences were considered statistically significant at $P \leq .05$ (*), $P \leq .01$ (**), $P \leq .001$ (***).

3. Results

Patient-specific 3D printed titanium cages were used in 5 consecutive patients (male 3, female 2) to reconstruct femoral post-traumatic segmental defects (Figs. 1–3), with a mean age of 49.0 years (26–73; patient demographics are summarized in Table 1). The defects were the result of Gustilo[26,27] Grade 3B open distal femoral fractures (AO/OTA 33C) in 3 cases (Figs. 1A and 3A and D), and followed debridement of femoral infected nonunions (Cierny-Mader[28] class 4B) in 2 patients (Fig. 3G and J). These were both actively draining and grossly infected at the time the first stage was undertaken. Culture specimens were obtained routinely at the start of the second stage according to the

Table 1

Patient demographics.

Patient	Age, years	Gender	Etiology	Side	Site	Fixation	Follow-up, months
A	53	F	Infected nonunion	Right	D	IM nail	33
B	37	M	Open fracture	Right	MD	ORIF	22
C	56	M	Open fracture	Right	MD	ORIF	25
D	73	F	Infected nonunion	Left	MD	ORIF	17
E	26	M	Open fracture	Right	D	IM nail	12
Mean	49.0	M3–F2	Open fx 3 INU 2	R4–L1	D2-MD3	ORIF 3 - IM nail 2	21.8

D = diaphyseal, MD = meta-diaphyseal, ORIF = open reduction internal fixation.

treatment protocol, and returned negative in all 5 of these cases. There was a mean interval between stages of 100.2 days (83–119; characteristics of the defects are summarized in Table 2). The mean defect measured 14.0 cm (10.3–18.4) in length. The mean bone defect volume was 192.4 cc (114–292). During the first stage the defect was filled with antibiotic PMMA closely approximating the contours of the missing bone, stabilized with an IM nail in 2 cases, and a lateral locked distal femoral plate in 3 cases. After returning for the second stage the fixation was modified as necessary, but otherwise remained the same.

The mean length of follow-up was 21.8 months (12–33). There were no deep infections, fractures, nerve injuries, loss of alignment, or nonunions identified during the period of follow-up. All of the patients (5/5) achieved union clinically and radiographically (Figs. 1–3); clinical outcomes are summarized in Table 2. Long-standing AP radiographs when last reviewed

Figure 3. Case series radiographs. (A–C) 37 year old male sustained polytrauma in a high-speed motor vehicle accident, with injuries including a Grade 3A open comminuted intra-articular right distal femur fracture with 15 cm bone loss and associated articular cartilage deficits; (A) initial injury AP radiograph after preliminary debridement and spanning external fixation; (B) AP radiograph 9 months following staged reconstruction using a patient-specific 3D printed titanium cage placed into a Masquelet-induced membrane, demonstrating incorporation of the implant with a solid column of bone bridging the defect medially; (C) lateral radiograph further confirming incorporation of the implant with additional bone bridging the defect posteriorly. (D–F) 26 year old male sustained polytrauma in a high-speed motorbike accident, with injuries including a Grade 3B open comminuted right diaphyseal femur fracture with 11 cm bone loss; (D) initial injury AP radiograph after preliminary debridement and spanning external fixation; (E) AP radiograph 7 months following staged reconstruction using a patient-specific 3D printed titanium cage placed into a Masquelet-induced membrane, demonstrating osseointegration of the implant at both the proximal and distal junctions; (F) lateral radiograph further confirming incorporation of the implant with a very solid column of bone bridging the defect posteriorly. (G–I) 73 year old female sustained a closed intra-articular left distal femur fracture in a motor vehicle accident, which developed into an infected nonunion within 3 months following internal fixation; (G) initial referral AP radiograph with persistent infection following preliminary debridement, with antibiotic PMMA beads laterally; (H) AP radiograph 6 months following staged reconstruction using a patient-specific 3D printed titanium cage placed into a Masquelet-induced membrane, demonstrating incorporation of the implant with a solid column of bone bridging the defect medially; (I) lateral radiograph illustrating incorporation of the implant with no change in position or alignment relative on serial radiographs. (J–L) 53 year old female who developed an infected nonunion of the right femoral diaphysis following multiple attempts to address a 7 cm post-traumatic LLD; (J) AP radiograph demonstrating Cierny/Mader 4B chronic osteomyelitis with collapse of a prior intercalary allograft; (K) AP radiograph 6 months following staged reconstruction using a patient-specific 3D printed titanium cage placed into a Masquelet-induced membrane, suggesting early incorporation at the host–implant junction proximally and distally; (L) lateral radiograph better demonstrating incorporation at the host-implant junction proximally and distally.

Table 2

Defect characteristics and clinical outcomes.

Patient	Defect length, cm	Defect volume, cc	Interval between stages, days	Volume of bone graft required, cc	Coronal deformity, degrees	Leg length discrepancy, mm	Range of motion, degrees
A	15.2	187	119	123	0.1 valgus	2 mm long	0–120
B	15.1	248	85	155	1.9 varus	9 mm short	0–115
C	18.4	292	108	239	2.2 valgus	23 mm short	10–75
D	10.3	114	106	77	1.4 varus	0 mm	0–110
E	11.1	121	83	72	1.0 valgus	6 mm short	0–100
Mean	14.0	192.4	100.2	133.2	1.3	8	2–104

demonstrated coronal plane mechanical femoral-tibial angulation of less than 3° in all 5 patients; there was a mean residual coronal lower extremity mechanical axis angulation of only 1.3° (1.9°–2.2° valgus). There was a mean residual leg length discrepancy (LLD) of 8 mm (2–23), with 3/5 measuring less than 7 mm. Mean knee flexion at latest follow-up measured 104° (75°–120°). Mean knee extension at the latest follow-up measured 2° (0°–10°), with just 1 patient not achieving full extension. The only patient with significant loss of motion (10–75° range of motion) had the largest defect (18.4 cm), and needed a medial gastrocnemius myoplasty to cover an open knee; the other 4 patients all achieved full extension and 100° or more flexion. At latest follow-up all 5 were ambulating, full weight bearing, and pain free, with 1 patient using a cane when ambulating distances.

Complications included the limitation of knee range of motion in one patient, as described above. There was one instance of a superficial stitch abscess that responded immediately to a week of oral antibiotics. Several locked screws disengaged from a plate in one case within 6 weeks, and were revised uneventfully. During the second stage 1 patient became acutely hypotensive while reaming the opposite femur to obtain bone graft, when the femur was inadvertently not vented prior. The procedure was discontinued and the patient transferred to intensive care, and the case was completed successfully the following week.

3.1. Histology

Quantitative histology, H&E, and Masson Trichrome staining of local fascia (control) and induced membrane samples were used to evaluate differences in tissue morphology. The results demonstrated that the local fascia had a well-organized structure with highly oriented dense layers of undulated collagen fascicles (Fig. 4A and A1). It also showed very low density of mature blood vessels and elongated cells (Fig. 4B1), which were mostly

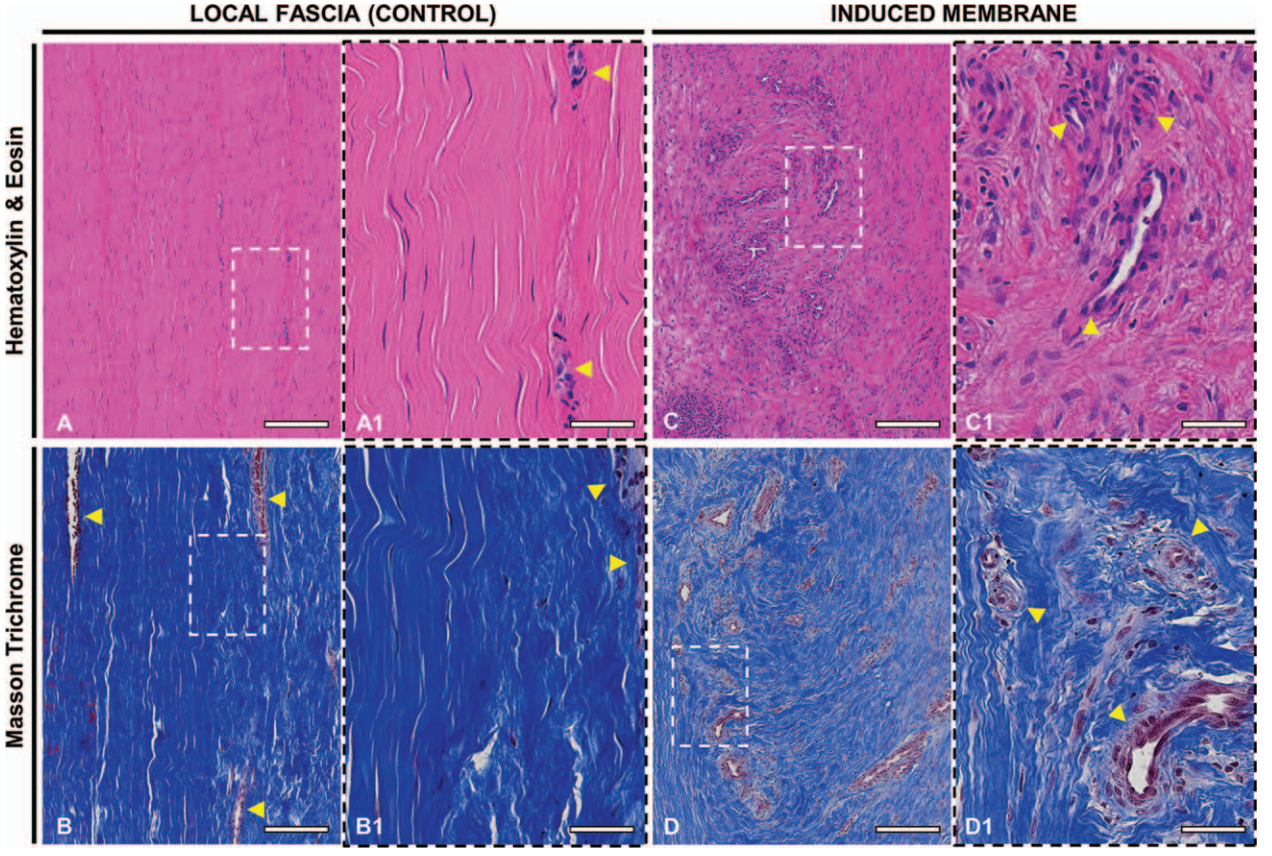

Figure 4. Morphology of local fascia (control) and induced membrane tissues were evaluated using H&E and Masson Trichrome stains. (A, A1) H&E staining, and (B, B1) Masson Trichrome staining of local fascia. (C, C1) H&E staining, and (D, D1) Masson Trichrome staining of an induced membrane. Yellow arrows indicate mature blood vessels in A, A1, B, and B1, and mature blood vessels, microvessels, and capillaries in C, C1, D, and D1. Scale bar in A–D 200 μm, in A1–D1 50 μm.

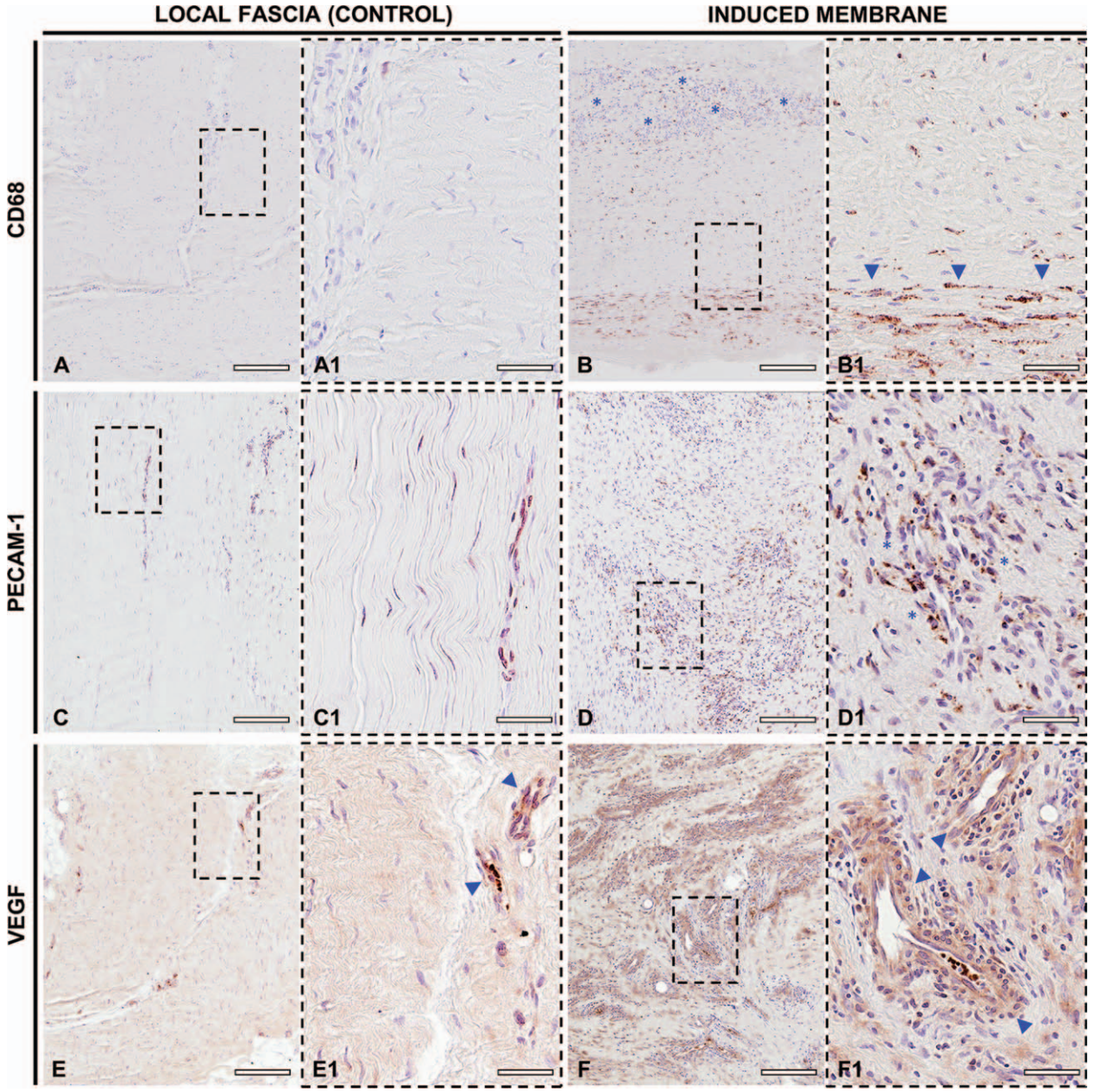

Figure 5. Immunohistochemical localization of CD68, PECAM-1, and VEGF in local fascia (control) and induced membrane tissues. (A, A1) CD68 staining of local fascia was negative for CD68 cells. (B, B1) CD68 staining of an induced membrane, indicate areas of high cell and vascular density (blue asterisks in B) and a distinct layer of CD86 positive cells (blue arrows in B1). (C, C1) PECAM-1 staining of local fascia. (D, D1) PECAM-1 staining of an induced membrane, indicate vascularized areas of the membrane (blue asterisks). (E, E1) VEGF staining of local fascia, indicate VEGF-positive vascular structures (blue arrows). (F, F1) VEGF staining of an induced membrane, show VEGF staining around the blood vessels (blue arrows). Scale bar in A-F 200 μm, in A1-F1 50 μm.

fibroblasts and myofibroblasts. In contrast to the fascia, the induced membranes were structurally disorganized (Fig. 4C and C1). They consisted of a collagenous matrix (Fig. 4D and D1) that contained a combination of mature vessels, microvessels, and capillaries densely distributed throughout the tissue. All induced membranes exhibited a strikingly higher cell density, especially in highly vascularized areas of the membranes.

Immunohistochemistry showed that fascia controls were negative for CD68, which is a marker for macrophages (Fig. 5A and A1).[29] In contrast, CD68 was expressed throughout all induced membranes, especially in areas of high cell and vascular density (Fig. 5B). Interestingly, the cross-section showed a very distinct layer of CD68-positive cells immediately adjacent to the PMMA spacer (Fig. 5B1). PECAM-1, also known as CD31, is a cellular adhesion, signaling, and angiogenic marker molecule, which is expressed on endothelial cells and platelets. Previous studies have shown that PECAM-1 is also constitutively expressed in macrophages and plays a role in inflammation.[30,31] In this study, PECAM-1-positive cells were found in both the local fascia (Fig. 5C and C1) and the induced membranes (Fig. 3D), which showed more intense staining around the vascularized areas of the membranes (Fig. 5D1). VEGF, a secreted angiogenic mitogen regulating endothelial cell growth and differentiation factor,[32] was expressed around blood

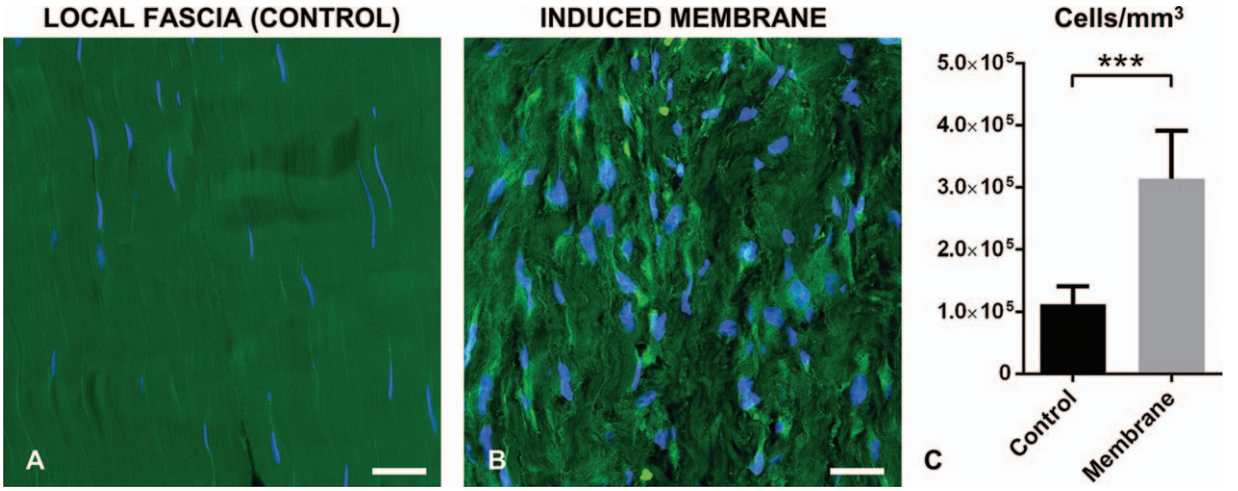

Figure 6. Cell density in local fascia (control) and induced membrane tissues. (A) Representative image of local fascia (control). (B) Representative image of an induced membrane. Cell nuclei are visible in blue (DAPI), tissues in green (autofluorescence). (C) Quantitative analysis of the cell numbers per mm^3. Bars represent the mean ± SD. $^{***}P \leq 0.001$; n = 5. Scale bar = 50 μm.

vessels of both local fascia (Fig. 5E and E1) and induced membranes (Fig. 5F and F1).

3.2. Analysis of cell density

The average cell density was quantified in both the control and induced membrane samples by counting cell nuclei in DAPI stained sections (Fig. 6A and B). This analysis revealed an average cell density of 1.12 (± 0.26) × 10^5 cells/mm^3 in local fascia and 3.14 (± 0.69) × 10^5 cells/mm^3 in the induced membranes, which resulted in a 2.8-fold ($P = .0006$, n = 5) higher cell number in the membrane samples (Fig. 6C).

3.3. Gene expression analysis

The differential expression of genes from angiogenic, osteogenic, and inflammatory pathways was measured in the induced membranes relative to the local fascia (Fig. 7). Consistent with the results of the IHC stains, the gene expression analysis demonstrated a 3.3-fold upregulation of VEGFA, which is essential for angiogenesis. Furthermore, induced membranes had a 5.9-fold upregulation of ANG, a potent mediator of new blood vessel formation. In contrast, platelet derived growth factor A; important for wound healing, VEGF-B, and von Willebrand factor; promotes adhesion of platelets to the sites of vascular injury, were downregulated compared to local fascia by 8.7-fold, 2.7-fold, and 2.2-fold, respectively (Fig. 7A). Osteogenic activity of the induced membrane was demonstrated by a 152.8-fold upregulation of TGF-ß1, which is an important stimulator of osteoblastic bone formation. RUNX2 was also upregulated by 7.5-fold, which is essential for the maturation of osteoblasts, whereas secreted phosphoprotein 1, a gene involved in the attachment of osteoclasts to the mineralized bone matrix, was downregulated by 6.1-fold. BMP-2, an important regulator of bone development, was upregulated by 2.1-fold in the induced membranes, whereas BMP-4 and BMP-6 were downregulated by 2.5-fold and 4.4-fold, respectively. COL1-A1 (collagen type I alpha 1; −2.1-fold), abundant in bone, GDF-5 (+3.6-fold) and GDF-10 (+2.3-fold), both involved in osteoblast and bone formation, as well as TGF-ß3 (−4.3-fold), which plays a key role in wound healing, were significantly up- or downregulated in the induced membranes (Fig. 7B). Likewise, inflammatory genes, like IL-6, had a 5.8-fold increased expression, which is essential for the final differentiation of B-cells. NF-κB1, involved in immune cell development, was upregulated by 28.1-fold. RANKL, affecting the maturation and activation of the immune system and a key factor for osteoclast differentiation, was upregulated by 6.9-fold in the induced membranes compared to the local fascia. interleukin-1B, another important mediator of the inflammatory response, was downregulated by 3.9-fold (Fig. 7C).

4. Discussion

Management of large bone defects often requires multiple surgeries, and most techniques used for limb reconstruction are therefore associated with lengthy treatment times, unpredictable union rates, or methods that are poorly tolerated by patients.[1,3,13] The main purpose of this study was to introduce a novel means to manage the extremely difficult problem of post-traumatic segmental bone loss, using patient-specific 3D printed titanium cages in conjunction with the Masquelet technique. The principal aims were to assess the clinical utility of this approach, and to evaluate the biological activity of the induced membranes, along with its potential influence on the initiation of bone defect healing.

Previous case reports have already supported the use of patient-specific 3D printed cages, with promising outcomes for these challenging cases. Most of these have involved smaller defects in the foot,[33,34] or the cages were used for ankle arthrodesis.[35–37] Several publications describe the reconstruction of long bones, including Herry et al.[38] who salvaged a tibial diaphyseal defect using a solid implant into an induced membrane. Hamid et al.[39] reconstructed a large distal tibial defect by inserting an implant very similar to those reported here into an induced membrane. Finally, Pobloth et al.[40] described cases most similar to this series, reconstructing 2 large femoral defects with custom cages placed into an induced membrane. Although reporting few clinical details, they did note one implant failure after 8 months.

The preliminary outcomes described here represent the largest series of cases ever reported using this approach, and suggests the

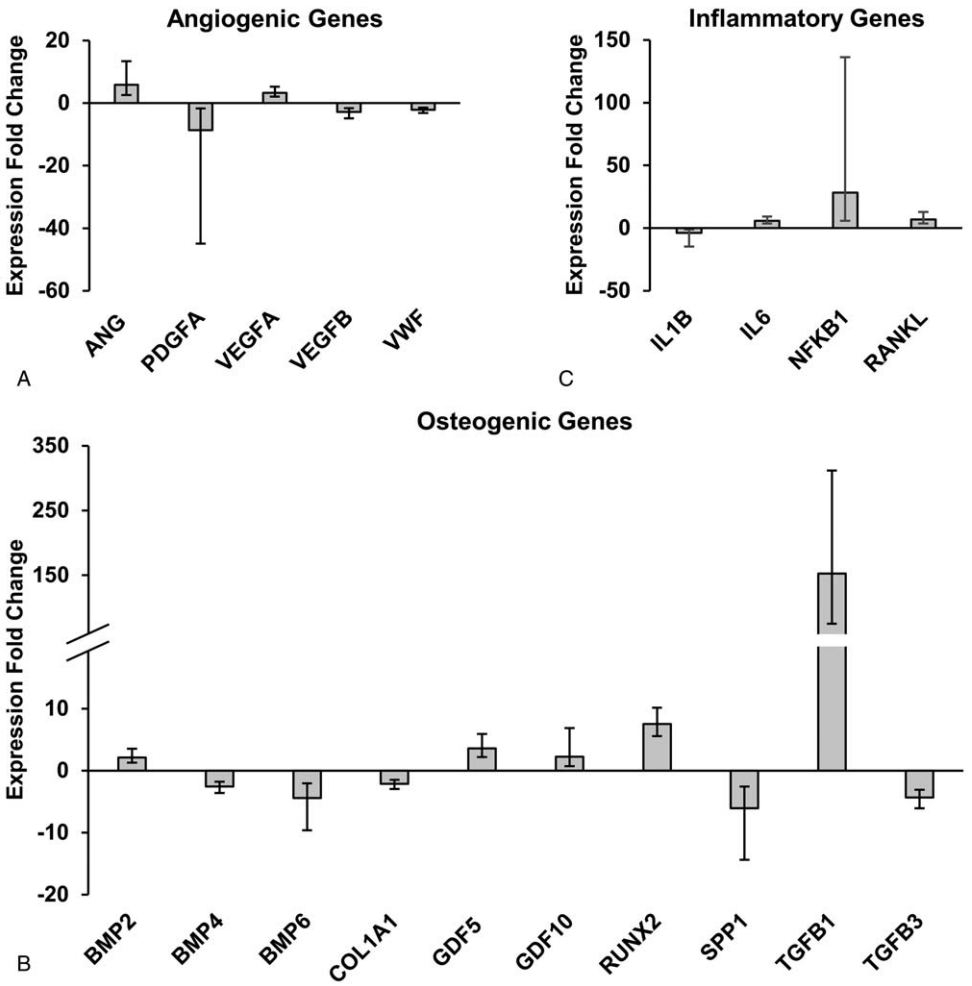

Figure 7. Gene expression analysis, induced membrane relative to local fascia (control). (A) Angiogenic genes: ANG, PDGFA—platelet-derived growth factor A, VEGFA and VEGFB A and B, VWF—von Willebrand factor. (B) Osteogenic genes: BMP-2, BMP-4, and BMP-6, collagen Type I alpha 1, GDF-5 and GDF-10, RUNX2, SPP1—secreted phosphoprotein 1, TGF-ß1 and TGF-ß3. (C) Inflammatory genes: interleukin 1 beta and IL-6, NF-κB1, RANKL. Expression fold change ± range, n = 3, housekeeping gene: B2M (beta-2-microglobulin). Fold change > 2 or < -2; $^{*}P \leq .05$.

use of custom 3D printed titanium cages, in conjunction with the Masquelet technique, holds genuine potential as another treatment option for managing complex segmental bone loss. The mechanical and structural stability of these constructs facilitated immediate motion and early weight bearing. The staged approach was crucial, and played a critical role in the success of the procedure. This allowed the soft tissues to recover completely, while also providing the time necessary to complete the required additional processes of custom implant design, manufacture, sterilization, and delivery.[17] Placing these titanium cages into the highly favorable environment created by an induced membrane consistently resulted in stable osseous integration of the implants in this small series.

The favorable biological activity of the induced membrane was confirmed in biopsy specimens obtained during the second stage, consistent with prior publications.[14,23,24] Molecular analysis of the membranes revealed differential expression of various growth factors associated with the initiation of bone repair. This was most clearly demonstrated by the differential regulation of those genes involved in the inflammatory, angiogenic, and osteogenic pathways. For instance, VEGF, one of the most influential genes in the angiogenic pathway, was significantly upregulated compared to the local fascia controls, which is essential for blood vessel formation and osteoblast activation. This supports the findings of numerous studies, where VEGF was shown to stimulate the vascular endothelial cells to secrete growth factors and cytokines that influence the differentiation of mesenchymal cells to enter the osteogenic pathway and engage in osteogenesis.[41,42] Furthermore, the results of this study also showed that many osteogenic pathway related growth factors, including TGF-β1, BMP-2, GDF-5, GDF-10, and RUNX2, were significantly upregulated, confirming osteogenic activity. Notably, TGF-β1 had a 152.8-fold increase in the induced membrane compared to the local fascia, which plays an important role in stem cell activity, bone metabolism, and extracellular matrix protein synthesis.[43] The combined actions of these cellular responses mediate the effects of TGF-β1 on immune responses, angiogenesis, and bone formation. For example, a study by Tachi et al.[44] demonstrated that TGF-β1 strongly enhances the osteoinductive activity of BMP-2, consistent with the results of this study that revealed significantly increased levels for both of these genes. This response was further corroborated by the IHC results demonstrating extensive diffuse staining for CD68, localizing the distribution of osteogenic macrophages, as a marker of bone formation. This was also evident from the histological analysis of the biopsy specimens, where the findings confirmed a greater

number of vessels and cell nuclei distributed throughout the induced membrane relative to the local fascia.

Although preliminary, these results clearly indicate that the membranes harvested at 12 to 17 weeks remain highly biologically active, and most likely contribute in meaningful ways to the incorporation of bone in and around the titanium cages. In contrast, Aho et al.[23] reported that the biological activity of the membranes was the highest at one month, with 60% decreased vascularization from 1 to 3 months, and 40% lower expression of VEGF and Col-1 in 2 month old membranes. Likewise, Gruber et al.[24] also reported that membranes residing in the host longer than 3 months had only a modest upregulation of stem cell-related genes (BMP-7, fibroblast growth factor 4, sonic hedgehog), and a significant downregulation of the osteogenic genes (RUNX2, bone morphogenetic protein receptor 2, bone morphogenetic protein receptor 1A, matrix metallopeptidase 9). The reasons for these differences are not clear, but this could be related to the patients' age, the anatomical location, physiological status of the subjects, size of the defects, stability of the temporary constructs, and experimental setup in each study.[23–25] For example, Gruber et al. selected a human foetal osteoblast cell line as the control for the gene expression analysis while in this study local fascia was used, which makes a direct comparison impossible. Despite these discrepancies between studies, it is very evident that induced membranes are highly biologically active and influence the healing of bone defects.

The most significant limitation of this study was its observational nature, and is therefore susceptible to possible selection bias, performance bias, and recall bias. There was no comparative treatment group, and selection bias may have influenced the results reported here in a manner difficult to predict. The potential performance bias was introduced by having a single senior surgeon (KT) involved in all of these procedures, limiting the external validity of the results reported. Recall bias could have been introduced because complications may not have always been identified prospectively or recorded contemporaneously, and therefore could have been under reported. Another limitation of this study is that there was a small sample size of the membranes for the gene expression analyses, histology, and IHC. Although the differences in gene expression reached statistical significance, and the analysis of tissue morphology showed distinct differences between membrane and control samples, future studies with larger sample sizes are required.

5. Conclusions

This study demonstrates that the use of a patient-specific 3D printed custom titanium cage, inserted into an induced membrane in a 2-stage protocol, can achieve very acceptable clinical outcomes in selected cases of post-traumatic femoral segmental defects.[5–12] These constructs were most advantageous for cases of massive juxta-articular bone loss, when other biological techniques were considered unsuitable. This is a particularly appealing treatment option in younger patients because of the joint-preserving nature, and the facilitation of early weight bearing. Despite these encouraging early results, further work will be required to identify the appropriate indications and to define the limitations related to this approach.

Acknowledgments

We would like to thank Bridney Lundquist, BS, and Jesse Hernandez, MS, for their technical assistance with the histology, immunohistochemistry, imaging, and gene expression analysis.

References

1. DeCoster TA, Gehlert RJ, Mikola EA, et al. Management of posttraumatic segmental bone defects. J Am Acad Orthop Surg. 2004; 12:28–38.
2. Tetsworth K, Dlaska CE. The art of tibial bone transport using the Ilizarov fixator: the suspension wire technique. Tech Orthop. 2015;30: 142–155.
3. Tetsworth K, Paley D, Sen C, et al. Bone transport versus acute shortening for the management of infected tibial nonunions with bone defects. Injury. 2017;48:2276–2284.
4. Malizos KN, Zalavras CG, Soucacos PN, et al. Free vascularized fibular grafts for reconstruction of skeletal defects. J Am Acad Orthop Surg. 2004;12:360–369.
5. Coulet B, Pflieger JF, Arnaud S, et al. Double-barrel fibular graft for metaphyseal areas reconstruction around the knee. Orthop Traumatol Surg Res. 2010;96:868–875.
6. Dugan TR, Hubert MG, Siska PA, et al. Open supracondylar femur fractures with bone loss in the polytraumatized patient—timing is everything!. Injury. 2013;44:1826–1831.
7. Bosse MJ, MacKenzie EJ, Kellam JF, et al. An analysis of outcomes of reconstruction or amputation after leg-threatening injuries. N Engl J Med. 2002;347:1924–1931.
8. Karger C, Kishi T, Schneider L, et al. Treatment of posttraumatic bone defects by the induced membrane technique. Orthop Traumatol Surg Res. 2012;98:97–102.
9. Masquelet AC, Begue T. The concept of induced membrane for reconstruction of long bone defects. Orthop Clin North Am. 2010; 41:27–37.
10. Stafford PR, Norris BL. Reamer-irrigator-aspirator bone graft and bi Masquelet technique for segmental bone defect nonunions: a review of 25 cases. Injury. 2010;41 (suppl 2):S72–S77.
11. Taylor BC, French BG, Fowler TT, et al. Induced membrane technique for reconstruction to manage bone loss. J Am Acad Orthop Surg. 2012;20:142–150.
12. Appleton P, Moran M, Houshian S, et al. Distal femoral fractures treated by hinged total knee replacement in elderly patients. J Bone Joint Surg Br. 2006;88:1065–1070.
13. Pollak AN, Ficke JR. Extremity War Injuries IIISMExtremity war injuries: challenges in definitive reconstruction. J Am Acad Orthop Surg. 2008;16:628–634.
14. Giannoudis PV. Has the induced membrane technique revolutionized the treatment of bone defects? Tech Orthop. 2016;31:2.
15. Morris R, Hossain M, Evans A, et al. Induced membrane technique for treating tibial defects gives mixed results. Bone Joint J. 2017;99-B: 680–685.
16. Muhlhausser J, Winkler J, Babst R, et al. Infected tibia defect fractures treated with the Masquelet technique. Medicine (Baltimore). 2017;96: e6948.
17. Tetsworth K, Block S, Glatt V. Putting 3D modelling and 3D printing into practice: virtual surgery and preoperative planning to reconstruct complex post-traumatic skeletal deformities and defects. SICOT J. 2017;3:16.
18. Cobos JA, Lindsey RW, Gugala Z. The cylindrical titanium mesh cage for treatment of a long bone segmental defect: description of a new technique and report of two cases. J Orthop Trauma. 2000;14:54–59.
19. Gugala Z, Lindsey RW, Gogolewski S. New approaches in the treatment of critical-size segmental defects in long bones. Macromol Symp. 2007;253:147–161.
20. Lindsey RW, Gugala Z. Cylindrical titanium mesh cage for the reconstruction of long bone defects. Osteosynthesis Trauma Care. 2004;12:108–115.
21. Attias N, Thabet AM, Prabhakar G, et al. Management of extra-articular segmental defects in long bone using a titanium mesh cage as an adjunct to other methods of fixation. Bone Joint J. 2018;100-B:646–651.
22. O'Malley NT, Kates SL. Advances on the Masquelet technique using a cage and nail construct. Arch Orthop Trauma Surg. 2012;132: 245–248.
23. Aho OM, Lehenkari P, Ristiniemi J, et al. The mechanism of action of induced membranes in bone repair. J Bone Joint Surg Am. 2013; 95:597–604.
24. Gruber HE, Ode G, Hoelscher G, et al. Osteogenic, stem cell and molecular characterisation of the human induced membrane from extremity bone defects. Bone Joint Res. 2016;5:106–115.
25. Pelissier P, Masquelet AC, Bareille R, et al. Induced membranes secrete growth factors including vascular and osteoinductive factors and could stimulate bone regeneration. J Orthop Res. 2004;22:73–79.

26. Gustilo RB, Anderson JT. Prevention of infection in the treatment of one thousand and twenty-five open fractures of long bones: retrospective and prospective analyses. J Bone Joint Surg Am. 1976;58:453–458.
27. Gustilo RB, Mendoza RM, Williams DN. Problems in the management of type III (severe) open fractures: a new classification of type III open fractures. J Trauma. 1984;24:742–746.
28. Cierny G3rd, Mader JT, Penninck JJ. A clinical staging system for adult osteomyelitis. Clin Orthop Relat Res. 2003;414:7–24.
29. Barros MH, Hauck F, Dreyer JH, et al. Macrophage polarisation: an immunohistochemical approach for identifying M1 and M2macrophages. PLoS One. 2013;8:e80908.
30. Rui Y, Liu X, Li N, et al. PECAM-1 ligation negatively regulates TLR4 signaling in macrophages. J Immunol. 2007;179:7344–7351.
31. Woodfin A, Voisin MB, Nourshargh S. PECAM-1: a multi-functional molecule in inflammation and vascular biology. Arterioscler Thromb Vasc Biol. 2007;27:2514–2523.
32. Breier G, Albrecht U, Sterrer S, et al. Expression of vascular endothelial growth factor during embryonic angiogenesis and endothelial cell differentiation. Development. 1992;114:521–532.
33. Coriaty N, Pettibone K, Todd N, et al. Titanium scaffolding: an innovative modality for salvage of failed first ray procedures. J Foot Ankle Surg. 2018;57:593–599.
34. So E, Mandas VH, Hlad L. Large osseous defect reconstruction using a custom three-dimensional printed titanium truss implant. J Foot Ankle Surg. 2018;57:196–204.
35. Hsu AR, Ellington JK. Patient-specific 3-dimensional printed titanium truss cage with tibiotalocalcaneal arthrodesis for salvage of persistent distal tibia nonunion. Foot Ankle Spec. 2015;8:483–489.
36. Mulhern JL, Protzman NM, White AM, et al. Salvage of failed total ankle replacement using a custom titanium truss. J Foot Ankle Surg. 2016; 55:868–873.
37. Dekker TJ, Steele JR, Federer AE, et al. Use of patient-specific 3D-printed titanium implants for complex foot and ankle limb salvage, deformity correction, and arthrodesis procedures. Foot Ankle Int. 2018;39: 916–921.
38. Herry Y, Reynaud O, Ferry T, et al. Intercalary diaphyseal endoprosthetic reconstruction for tibial septic nonunion in an elderly patient: A case report. Orthop Traumatol Surg Res. 2017;103:1217–1220.
39. Hamid KS, Parekh SG, Adams SB. Salvage of severe foot and ankle trauma with a 3D printed scaffold. Foot Ankle Int. 2016;37:433–439.
40. Pobloth AM, Checa S, Razi H, et al. Mechanobiologically optimized 3D titanium-mesh scaffolds enhance bone regeneration in critical segmental defects in sheep. Sci Transl Med. 2018;10:eaam8828.
41. Holmes DI, Zachary I. The vascular endothelial growth factor (VEGF) family: angiogenic factors in health and disease. Genome Biol. 2005;6:209.
42. Mayer H, Bertram H, Lindenmaier W, et al. Vascular endothelial growth factor (VEGF-A) expression in human mesenchymal stem cells: autocrine and paracrine role on osteoblastic and endothelial differentiation. J Cell Biochem. 2005;95:827–839.
43. Wu M, Chen G, Li YP. TGF-beta and BMP signaling in osteoblast, skeletal development, and bone formation, homeostasis and disease. Bone Res. 2016;4:16009.
44. Tachi K, Takami M, Sato H, et al. Enhancement of bone morphogenetic protein-2-induced ectopic bone formation by transforming growth factor-beta1. Tissue Eng Part A. 2011;17:597–606.